Available online at www.sciencedirect.com
SCIENCE DIRECT®
Journal of Electron Spectroscopy and Related Phenomena 143 (2005) 139–147
JOURNAL OF ELECTRON SPECTROSCOPY and Related Phenomena
www.elsevier.com/locate/elspec

Energy-filtering transmission electron microscopy on the nanometer length scale

Werner Grogger[a,*], Maria Varela[b], Roger Ristau[c], Bernhard Schaffer[a], Ferdinand Hofer[a], Kannan M. Krishnan[d,*]

[a] *FELMI, Research Institute for Electron Microscopy, Graz University of Technology, Steyrergasse 17, A-8010 Graz, Austria*
[b] *ORNL, Condensed Matter Sciences Division, 1 Bethel Valley Road, Oak Ridge, TN, USA*
[c] *Seagate Recording Media, Fremont, CA, USA*
[d] *Department of Materials Science, University of Washington, Box 352120, Seattle, WA, USA*

Received 20 November 2003; received in revised form 22 September 2004; accepted 22 September 2004
Available online 9 December 2004

Abstract

Energy-filtering transmission electron microscopy (EFTEM), developed about ten years ago, is now a routine analysis tool in the characterization of materials. Based on the physical principles of electron energy-loss spectrometry (EELS), but with the addition of in-column or post-column energy-filters, it forms images of microstructures using a narrow energy band of inelastically scattered electrons. Post-column energy-filters, developed commercially by Gatan (Gatan Imaging Filter, GIF) in the early 1990s, could be attached to nearly any TEM. Almost at the same time, the introduction of the EM-912 microscope with an integrated Ω-filter by Zeiss, made it possible to use in-column filters as well. These two developments made EFTEM possible on an almost routine basis. The operation of these filters is rather straightforward and it is now possible to acquire element specific images within a few minutes. However, the optimal setup for data acquisition, the judicious choice of experimental parameters to solve specific materials science problems and the interpretation of the results can be rather difficult. For best results, a fundamental knowledge of the underlying physics of EELS and a systematic development of the technical details is necessary. In this work, we discuss the current status of EFTEM in terms of spatial resolution and illustrate it with a few technologically relevant applications at the nanometer length scale.

Keywords: EELS; EFTEM; Spatial resolution; Elemental mapping

1. Introduction

Transmission electron microscopy (TEM) is an efficient tool to explore the microstructure of almost any kind of material provided an electron-transparent thin-foil sample that is representative of the microstructure of interest can be prepared. Nowadays, the technique has become even more important as the structural dimensions in many materials science applications are rapidly approaching the nanometer length scale and are beyond the spatial resolution limits of other methods. Analytical capabilities (energy dispersive X-ray spectrometry, EDXS, and electron energy-loss spectrometry, EELS) with spatial resolution in the nanometer and sub-nanometer range combined with structural information from high resolution phase contrast imaging (HRTEM) makes TEM an indispensable tool for researchers in the fields of semiconductors, ultra fine grain materials or thin films. Energy-filtering TEM (EFTEM) has proven to be the key tool for nanoanalytical applications, since it uses the rich information provided by the energy-loss spectrum in a spatially resolved manner. Even though energy-filtering helps to improve contrast/resolution for conventional TEM imaging/diffraction, the main application of EFTEM is now the

* Corresponding authors. Tel.: +43 316 8738323; fax: +43 316 811596 (W. Grogger)/+1 206 543 3100 (K.M. Krishnan).
E-mail addresses: werner.grogger@felmi-zfe.at (W. Grogger), kannanmk@u.washington.edu (K.M. Krishnan).

0368-2048/$ – see front matter © 2004 Elsevier B.V. All rights reserved.
doi:10.1016/j.elspec.2004.09.028

acquisition of maps that elucidate the spatial distribution of any feature in the EEL spectrum [1]. Typically, the spatial distribution of elements using inner shell excitations and the variation in chemical bonding can be obtained rapidly (i.e. within minutes) and at a spatial resolution approaching and, in some cases, surpassing the nanometer length scale. In this paper we review the status of EFTEM and demonstrate its capabilities using some examples of real-world applications in magnetic recording media, high T_C superconductor oxide heterostructures and semiconductor devices. In addition, the paper will also focus on the spatial resolution issue of this technique.

2. Experimental

2.1. Energy-filtering TEM (EFTEM)

Electron energy-loss spectroscopy – as the basis for EFTEM – is the analysis of the energy distribution of electrons that have passed through the specimen and interacted inelastically with it [1]. In addition to the composition, an EEL spectrum also contains detailed information about the electronic structure of the atoms in the specimen, which in turn reveals details of the nature of these atoms, their bonding, nearest-neighbor distances, and their dielectric properties. In order to measure the energy-loss spectrum in almost all cases a spectrometer with a magnetic prism as the dispersing element is used. For EFTEM there are currently two different alternatives. A dedicated EFTEM microscope with an in-column filter, the so-called "omega filter", was developed by Zeiss [2–4] and later by JEOL. Alternatively, post-column energy-filters are manufactured by Gatan (GIF) [5,6] and can be installed as an attachment on the exit surface of the electron-optical column of almost any TEM. Both types of energy-filters are devices, that can form an image with electrons of only a small energy range.

The inelastic scattering process in EELS is strongly localized and, hence, it may be used to obtain analytical information from a small specimen area. By using any spectral feature in an EEL spectrum the change of this feature's intensity can be monitored simultaneously (and, at high spatial resolution) over a broad area of the specimen.

Zero-loss filtering is done by simply selecting the electrons over a narrow energy window that includes only the zero-loss peak. The contribution of inelastically scattered electrons to an image or diffraction pattern leads to a blurring due to chromatic aberration. Zero-loss filtering removes the contribution of all inelastically scattered electrons to both images and diffraction patterns. This is more serious for thicker specimens; hence, zero-loss filtering will improve the contrast and the resolution of such images considerably.

If an energy window at a somewhat higher energy-loss is selected, the plasmon resonance peak that is proportional to the number density of valence electrons can be mapped. An efficient way to increase contrast significantly is to find an energy range where certain features can be clearly seen. For biological tissue, such *contrast tuning* can be maximized at an energy-loss just below the C–K ionization edge (around 250 eV) which reduces the contribution of C to the image.

The most extensive analytical use of energy-filters is for *core-loss imaging* and *elemental mapping*. The ability of an energy-filter to show a two-dimensional distribution of a specific element, albeit integrated over the thickness of the thin-foil specimen, makes it a powerful tool for analytical studies. In our work, all the elemental maps were acquired with a post-column energy-filter (GIF); therefore, this technique will be explained in some more detail in the next section.

It should be mentioned that when specific features in the electron loss near-edge structure (ELNES) are used for EFTEM a *chemical bond map is obtained*. This technique can be applied to several ionization edges, the only requirement being a usable feature. In the case of the C–K ionization edge, there is a clear difference between carbon in diamond and amorphous (or diamond-like) carbon, which was successfully used for imaging (e.g. [7,8]).

2.2. Acquisition of EFTEM images

The data presented here was either acquired on a Philips CM20/STEM with a LaB_6 cathode (FELMI, Graz) or on a Philips CM200/FEG with a Schottky field emission source (NCEM, Berkeley). Both microscopes were equipped with a Gatan Imaging Filter (GIF) and a 1024×1024 CCD (YAG scintillator). Most of the TEM bright field images were not binned; however, virtually all EFTEM maps used a binning of 2×2 resulting in 512×512 images for reasons of better statistics in the images. All EEL spectra and EFTEM images/maps were acquired using the Digital Micrograph software. All images were corrected for the CCDs dark current and gain variations. However, no correction was performed neither for the point spread function of the detector [9] nor image distortions arising from electron-optical aberrations of the energy-filter.

Several important issues were taken into consideration during data acquisition. Since the focus of an EFTEM image differs significantly from the focus of the elastic image [10,11], we always focused the images at an energy-loss between 100 and 200 eV. We also took into account considerations about the influence of the different angles [11], in particular the collection angle was carefully chosen to allow for optimum spatial resolution. Another important parameter is the width of the energy-selecting slit. This and the positions of the pre-edge and post-edge windows were chosen to maximize SNR values. Calculations of SNR as a function of the various acquisition parameters and their optimal values are discussed in the literature [11,12].

2.3. EELS background removal

Energy-filtering using core-loss ionization edges is a very efficient method to measure the chemical composition and

its spatial distribution in a specimen. By choosing an energy window around an ionization edge, elemental mapping can be performed yielding a signal that is correlated to the concentration of a certain element. This results in an elemental distribution map where the intensity distribution in the image can be correlated with the elemental concentration.

The elemental signal, however, is superimposed on other signals like diffraction contrast, thickness variations, elastic contrast, and a strongly varying background that contains no elemental information. The EEL background can be readily accounted for; so the first processing step usually involves a background removal procedure.

Two images, obtained with energy windows before and after the ionization edge of interest, can be divided to yield a *jump ratio image* [13–15]. Such a jump ratio image is not very sensitive to non-elemental variations arising from diffraction contrast but is capable of minimizing the influence of the background. However, specimen thickness variations may create non-elemental contrast in a jump ratio image, and these images cannot be used to quantitatively extract chemical compositions [15,16]. An advantage is that this process requires minimal mathematical processing of the data – compared to more sophisticated methods (see below), and therefore, the noise in the resulting jump ratio image is not substantially increased.

For extracting elemental concentrations from EFTEM images it is necessary to completely remove the background under an ionization edge in order to obtain the net edge signal (*elemental map*) [17,18]. In this case at least two images need to be recorded in front of the ionization edge. For the background usually a power-law shape is assumed: $I_{bkg} = AE^{-r}$, with an r value that typically lies in the range between 2 and 6.

Specific circumstances can make it necessary to use more sophisticated background calculations and extrapolation methods. For instance, if the data is noisy or if small elemental concentrations are to be detected, the three-window method may fail due to noise. This method also does not work if there is not enough space in front of the ionization edge to place the two pre-edge windows. Therefore a four-window method has been proposed [19] for the case of closely spaced edges. For certain elemental combinations this method has turned out to be extremely useful, such as the simultaneous detection of the O–K and Cr–L_{23} edges.

Other methods using more than three-windows and/or other background shapes (e.g. for low energy-losses) have also been proposed. However, the three-window technique is quite simple and yields sufficiently accurate results that can be used for quantification. Together with the two-window method (jump ratio images) it is the most commonly used procedure to eliminate the EELS background for energy-losses greater than 100 eV.

2.4. Quantification of EFTEM elemental maps

For the quantification of EFTEM images it is necessary to obtain the net edge intensity signal (i.e. elemental map) by accurately removing the background contribution. The quantification procedure of EFTEM elemental maps is almost identical to the way EEL spectra are quantified.

For an *absolute quantification*, the measured net signal under an ionization edge collected inside a collection angle β and within an energy range ΔE ($I_{edge}(\beta, \Delta E)$) is directly related to the number of scattering atoms per unit area N:

$$N = \frac{I_{edge}(\beta, \Delta E)}{I_{ZL}\sigma(\beta, \Delta E)}$$

where I_{ZL} represents the unscattered (zero-loss) intensity and σ is the partial scattering cross-section [1]. For the quantification one would acquire an elemental map at the ionization edge and divide it by a zero-loss filtered image and the appropriate ionization cross-section. This absolute quantification scheme works pretty well for biological and amorphous specimens [20,21]. However, diffraction contrast in crystalline samples will cause serious problems [22].

On the other hand, *atomic ratio images* can be obtained by using the above equation simultaneously for two elements A and B (*relative quantification*). For the quantification of elemental maps it offers the additional advantage of minimizing non-element specific effects, like diffraction contrast and thickness variations, since the division cancels them – at least partially – out

$$\frac{N_A}{N_B} = \frac{I_{edge,A}(\beta, \Delta E)}{I_{edge,B}(\beta, \Delta E)} \frac{\sigma_B(\beta, \Delta E)}{\sigma_A(\beta, \Delta E)} = \frac{c_A}{c_B}$$

gives the atomic concentration ratio of the elements A and B. The quantification in this case consists of the acquisition of two elemental maps and the determination of the appropriate ionization cross-sections [1,23].

The quantification of both EEL spectra and EFTEM elemental maps strongly rely on the accurate knowledge of the partial ionization cross-sections σ. Several models have been proposed for the calculation of σ like the hydrogenic model [24] and the Hartree–Slater model [25] both of which exist in various versions taking into account additional effects like white lines.

On the other hand, a more experimentally oriented approach has turned out to yield more accurate results, especially for heavier elements. Similarly to EDX spectrometry, sensitivity factors (k-factors) can be used for the EELS and EFTEM quantification and can be measured using standards with well defined composition [26,27]. This k-factor method is very well suited for the quantification of EFTEM elemental maps

$$k_{AB} = \frac{\sigma_B(\beta, \Delta E)}{\sigma_A(\beta, \Delta E)}$$

However, the tabulated cross-sections and k-factors for EELS cannot be directly used for EFTEM maps, since they are usually measured for rather large energy windows ($\Delta E > 50$ eV), whereas for EFTEM, ΔE is typically between 10 and 50 eV. These small energy windows are much more sensitive to changes in the near-edge fine structure and so results are ex-

pected to be less accurate. However, this can be accounted for by properly recalculating the *k*-factors from similar experimental EEL spectra [22].

In practice, the quantitative analysis of elemental distributions needs some experimental prerequisites: the exposure times, energy slit widths, and collection angles for both image series must be known, and the illumination conditions of the TEM must not be changed in between the acquisition. Especially, the latter might impose a severe limitation, when for instance widely spaced edges are used, where a reduction of beam intensity might be advantageous. To get around this, one can even go a step further and neglect all differences in acquisition parameters. In this case, the quantification is only possible with the help of "external" quantitative information from either an EDX or EEL spectrum or if the overall composition or the composition of a particular region is accurately known (e.g. [43]).

2.5. Spatial resolution in EFTEM images

The spatial resolution obtained in an EFTEM image is influenced by the specific details of the experiment itself: the energy and the shape of the ionization edge of interest, experimental parameters such as the collection angle, the energy-selecting slit width, and the exposure time, and instrumental parameters (e.g. aberrations of the TEM objective lens, high voltage). Additionally, there are other experimental factors that also influence the spatial resolution such as specimen drift, radiation damage, characteristics of the electron detector (point spread function), instrumental instabilities (energy drift) and the electron dose that the electron source can deliver onto the specimen. There are a number of different ways to compute EFTEM spatial resolution that are described in the literature. The problem can be treated from a purely statistical point of view [28] provided the signal has a minimum magnitude compared to noise in order to reveal details in the image. Other authors calculate the contributions of chromatic aberration, delocalization of the inelastic scattering process, spherical aberration and the diffraction limit separately and then sum them quadratically [29,30].

When doing EFTEM at high magnifications elastic contrast (similar to an HRTEM image) that is always present in EFTEM images may become visible. As mentioned before, the goal of EFTEM using core-loss ionization edges is the visualization of pure elemental/chemical contrast. A detailed analysis of the effect of elastic contrast transferal to inelastic EFTEM images was done by Navidi-Kasmai and Kohl [31]. They found that for crystalline specimens elastic contrast in EFTEM images is unavoidable and increases with increasing specimen thickness. Furthermore, a reliable image contrast interpretation is only possible by comparing the experimental images with simulated ones. However, simulations seem to be only possible for thin specimens. A rough method for checking the contrast in a jump ratio image is to calculate another jump ratio using the two pre-edge images. If this pre-edge jump ratio image does not show any contrast and the real jump ratio image does, the contrast can be assumed to be element specific only. However, this question cannot be easily solved for elemental maps, since elastic contrast is not cancelled in elemental maps.

3. Results

3.1. High T_C superconductor multilayers

In many materials science applications it is known that thin films often exhibit physical properties different from those of bulk samples. In addition, these properties may be strongly influenced by their growth mechanisms. For example, many fundamental studies of high T_C superconductors (like the nature of superconductivity itself) are based on the measurement of ultrathin layers. In this example, we describe EFTEM imaging methods to understand the growth mechanism of complex, ionic oxides exhibiting superconductivity. Epitaxial $YBa_2Cu_3O_{7-x}$ (YBCO) and $PrBa_2Cu_3O_7$ (PBCO) multilayer stacks were investigated to distinguish between the two competing growth models that have been proposed: (a) layer-by-layer growth mode where each atomic layer grows independently [32,33], and (b) block-by-block growth mode where enough material must be present for a whole unit cell to nucleate [34]. Reports have been presented in recent years supporting both layer-by-layer [35] and block-by-block growth [36,37].

In order to answer the fundamental question of the growth mode of these cuprates, an extensive EFTEM study was carried out to complement previous X-ray diffraction and resistivity measurements [38]. For this reason, epitaxial $[YBCO_n/PBCO_5]_{100\,nm}$ superlattice multilayer stacks were grown on (1 0 0) $SrTiO_3$ in a high pressure sputtering system. In order to find out the appropriate growth model, a multilayer stack with a non-integer *n* was fabricated. For example, for $n \sim 1.5$, the two different growth models should yield different resulting stacks: a layer-by-layer growth will result in a more or less random fluctuation of Y atoms (i.e. solid solution or alloy) in the last deposited layer. However, for the block-by-block model the basic growth unit is a whole unit cell, yielding an island-like coverage (Fig. 1).

Whilst previous X-ray diffraction measurements had been interpreted in terms of a block-by-block growth model, we decided to provide a real space verification using EFTEM. Therefore, jump ratio images of Y and Pr were acquired using the low-loss ionization edges of both elements (Pr–N_{45} at 113 eV and Y–M_{45} at 157 eV). The results clearly revealed a block-by-block growth of these materials by finding the island-like growth depicted in Fig. 1 [39]. A spatial resolution value of 0.9 nm was estimated in this particular experiment (Fig. 2). The same technique was also used to investigate a couple of $[YBCO_n/PBCO_5]_{100\,nm}$ superlattice multilayer stacks with different *n*. These EFTEM results combined with results from other methods (HRTEM, X-ray diffraction, atomic force microscopy) were used to obtain information

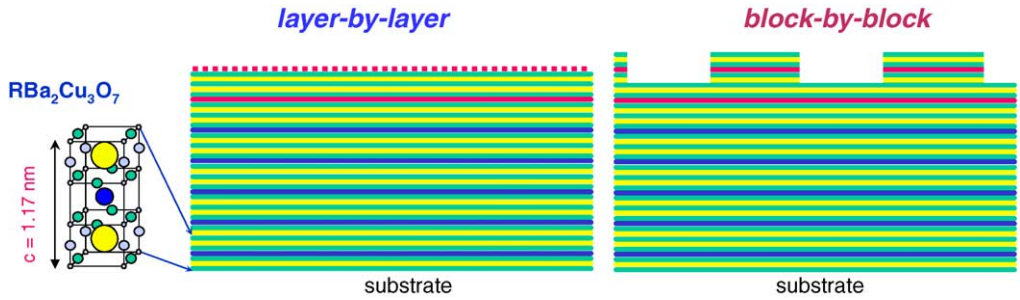

Fig. 1. Schematics of a layer-by-layer (left) and a block-by-block (right) growth mode for a $[YBCO_{1.5}/PBCO_5]_{100\,nm}$ multilayer stack consisting of nominally 1.5 unit cells of YBCO and five unit cells of PBCO.

on the epitaxial strain and the interface roughness of these multilayers [40,41].

3.2. Cr segregation in magnetic recording media

For the magnetic recording industry, the composition of the magnetic thin film recording media is paramount, as it influences their recording performance. In this application, commercial Co–Cr high density recording media were investigated by means of EFTEM to obtain information on the segregation of Cr to the grain boundaries. In this media, substantial segregation of Cr to the grain boundaries to create a non-magnetic phase is desirable. Rendering the local grain boundary phase non-magnetic (i.e. local Cr content > 24 at.%) is believed to strongly break the exchange coupling between individual, Co-rich, magnetic grains and decrease media noise at high recording densities. Therefore, it is critically important to measure the amount of Cr at the grain boundaries at statistical significance.

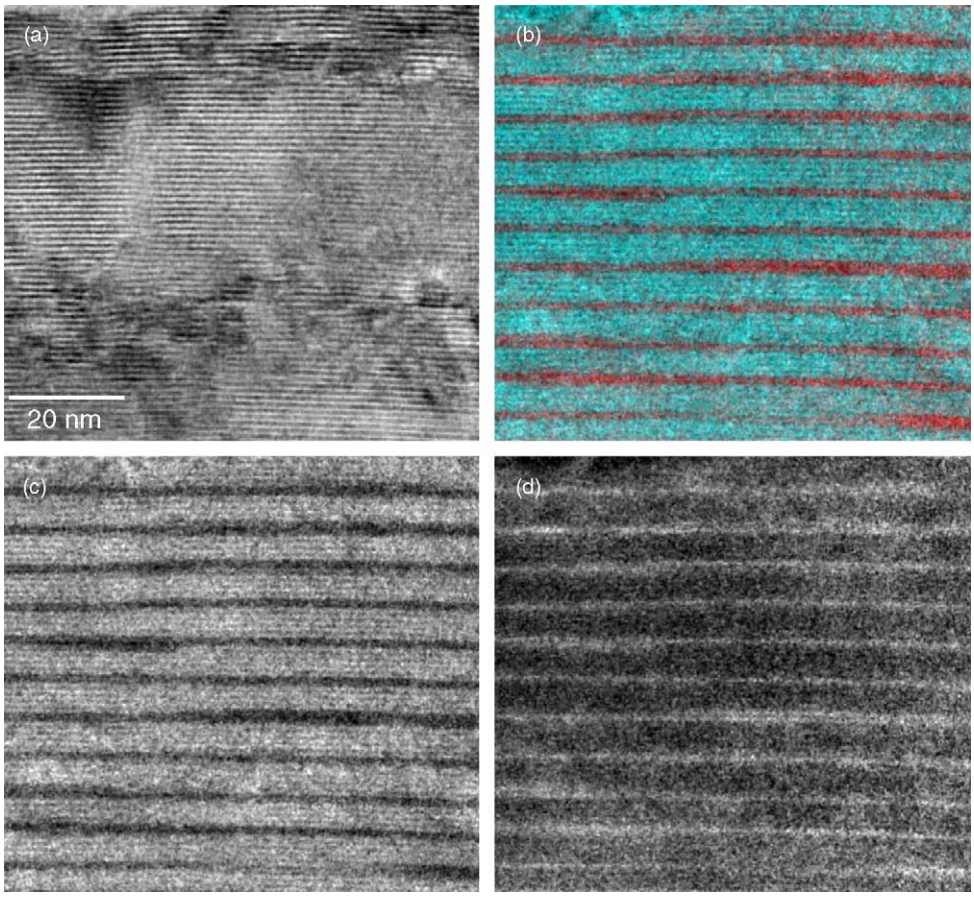

Fig. 2. EFTEM series of a $[YBCO_{1.5}/PBCO_5]_{100\,nm}$ multilayer. (a) TEM bright field image, (b) RGB image composed from (c) and (d), (c) Pr–N_{45} jump ratio image, (d) Y–M_{45} jump ratio image. In (b) and (d) areas can be seen that are only one unit cell high, whereas there are other areas showing two unit cell high layers. This stepwise behavior clearly indicates a block-by-block growth of YBCO.

The spatial resolution required in this kind of experiment is quite small. The typical grain diameter of magnetic recording media is in the 10 nm range and so the Cr segregation region at the grain boundaries is expected to be on the sub-nm scale. Additional constraints in this case included the very small specimen thickness of about 15 nm (i.e. media film thickness). Such ultrathin specimens correspond to an average of just 10 Cr atoms that contribute to the signal in one pixel of the EFTEM image recording device (slow-scan CCD). In addition to imaging the Cr inhomogeneities, the images needed to be quantified in order to obtain their chemical composition and to determine the Cr enrichment at the grain boundaries. The scatter diagram technique [42] turned out to be a very helpful method for dealing with such noisy signals and extracting quantitative information.

The results for two different CoCrPtB alloy compositions (10 and 16 at.% Cr content) are shown in Figs. 3 and 4. The segregation of Cr was quantitatively analyzed and the distribution of the non-magnetic phases with 24 at.% Cr or more visualized (Figs. 3d and 4d). It could be shown that almost all grains in a higher Cr content alloy were at least partially surrounded by the non-magnetic phase (Fig. 3), whereas in the lower Cr content sample (Fig. 4) the non-magnetic phase covered only a tiny fraction of the images (around 0.05%). This was correlated with recording performance [43,44].

3.3. SiO_2 layer in a semiconductor device

The final example in this work deals with the detection and the width measurement of thin silicon oxide layers used as gate oxides in semiconducting devices. As signal processing speed in these devices requires very thin gate oxide layers spatial resolution is again an issue. In most cases, HRTEM images do not show any difference in contrast between Si and the gate oxide layer, so the elemental signals obtained by EFTEM can be used. However, the use of elemental mapping using core-loss edges (O–K, Si–K) is limited due to the low signal-to-noise ratio. Therefore, the contrast in the low energy-loss region was systematically investigated between 10 and 99 eV right in front of the Si–L_{23} ionization edge [45,46]. This way, contrast maps were plotted as a function of energy-loss and specimen thickness. Two ideal regions were found, that show contrast almost independent of specimen thickness: 18 eV (5 eV slit width) and 80 eV (20 eV slit width).

After these findings, the question was raised whether it would be possible to measure layer widths from EFTEM im-

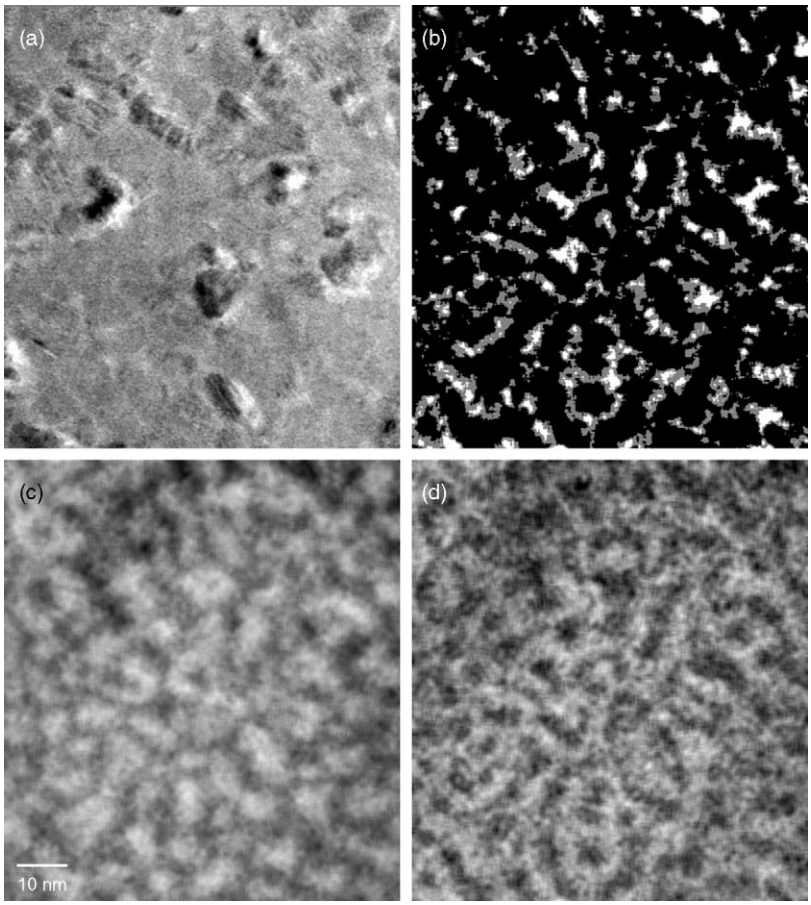

Fig. 3. EFTEM series of a Co–16Cr–10Pt–10B alloy. (a) TEM image, (b) map showing areas with more than 24 at.% Cr, (c) Co elemental map, (d) Cr elemental map.

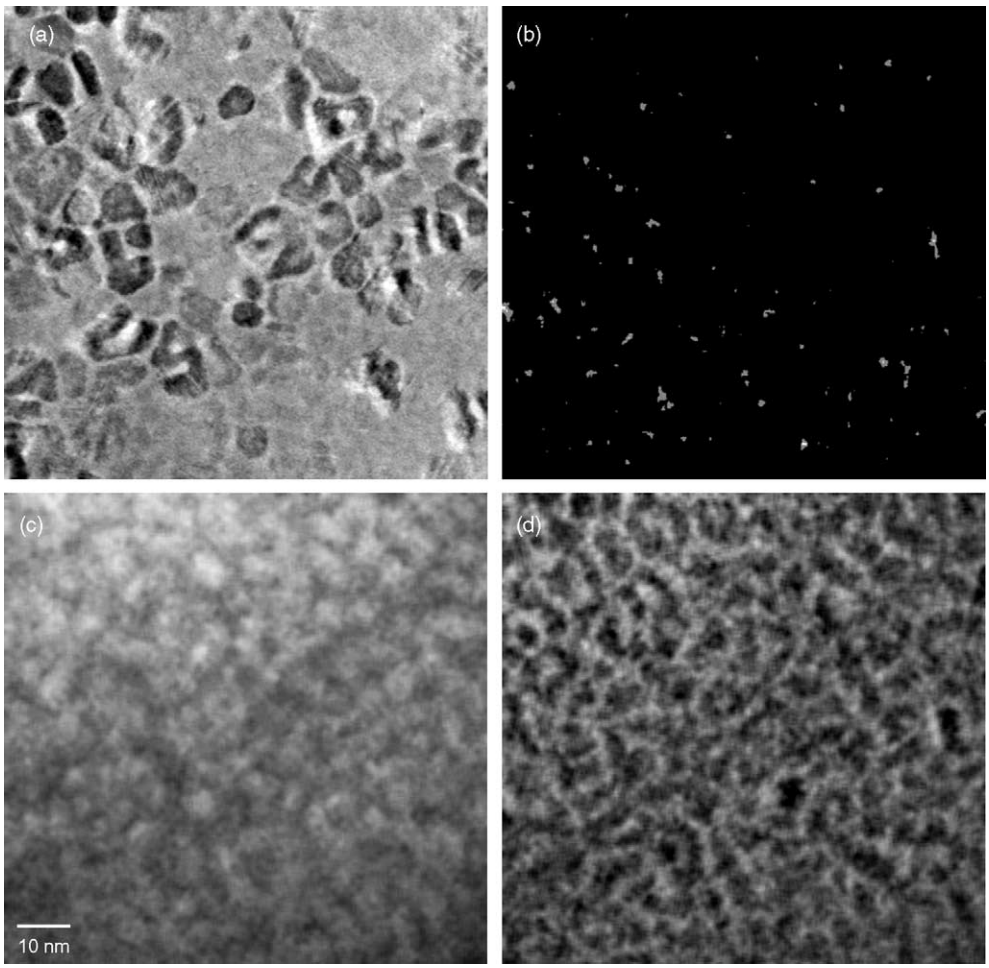

Fig. 4. EFTEM series of a Co–10Cr–10Pt–10B alloy. (a) TEM image, (b) map showing areas with more than 24 at.% Cr (compare with Fig. 3b (c) Co elemental map, (d) Cr elemental map.

ages that were acquired at low energy-losses. From the theoretical calculations it was clear that delocalization is the main factor determining EFTEM spatial resolution in this energy regime and yields resolution values between 4 and 5 nm (at 18 eV) [29,30].

However, the experiments for a 1.5 nm silicon oxide layer revealed a measured layer thickness at 18 eV of just 1.6–1.7 nm corresponding to a spatial resolution of about 1 nm [46]. The corresponding EFTEM images at 18 and 80 eV energy-loss are shown in Fig. 5, with their lineprofiles presented in Fig. 6. The discrepancy seems to lie in the formulae that are used for calculating the delocalization. Ref. [29] uses a formula from [47] that was later replaced by another description [48] yielding much smaller delocal-

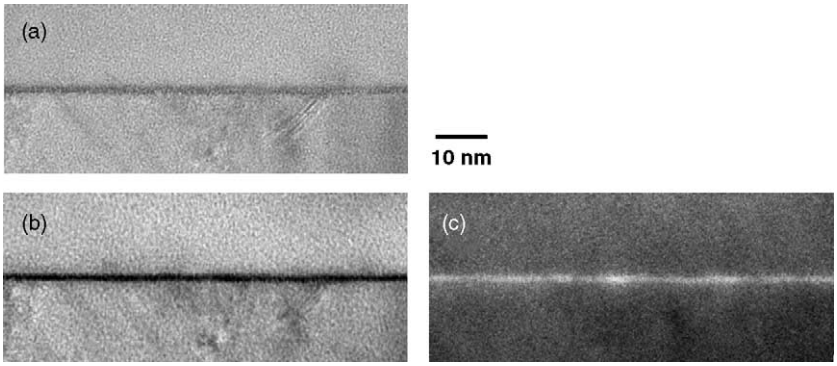

Fig. 5. EFTEM series of a 1.5 nm thin SiO_2 layer. (a) TEM bright field, (b) EFTEM image at 18 with 5 eV slit width, (c) EFTEM image at 80 eV with 20 eV slit width.

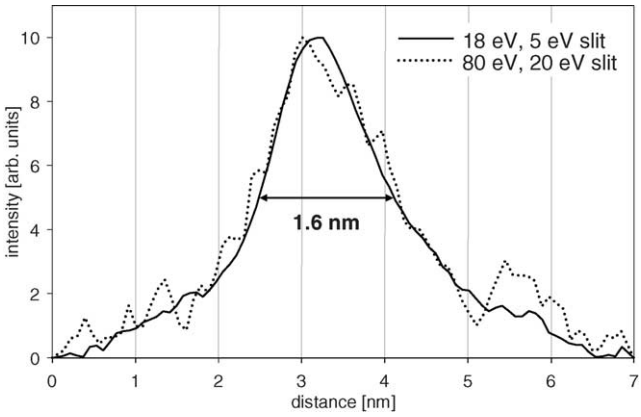

Fig. 6. Lineprofiles across the EFTEM images from Fig. 5b and c integrated over 100 pixels. The measured layer width at 18 and 80 eV is equal (approximately 1.6 nm) [46].

ization values around 0.1 nm. On the other hand, there are other reports stating that the effect of delocalization is often overestimated and in practice much smaller than expected [49]. These authors calculated delocalization values of about 0.5 nm which corresponds nicely to our results.

It should be noted that the influence of delocalization on spatial resolution is an example where a single value (e.g. FWHM or d_{50}) is not at all sufficient to describe the convolution curve. In many cases the assumption of a Gaussian or similar "simple" form of blurring is quite reasonable and the effect can be accurately described by a single number. However, the convolution caused by delocalization is not of a Gaussian shape, as there is a lot of intensity located in the extended tails of the intensity distribution. This topic is the subject of ongoing investigation in our group and elsewhere.

4. Conclusions

This work tries to highlight the current status of EFTEM in terms of spatial resolution and its direct applicability to materials science problems. It gives an overview about quantitative EFTEM at high spatial resolution. The important issues when going to high magnifications are discussed and practical application examples are described in order to demonstrate the capabilities of the technique.

Acknowledgements

The authors are thankful to G. Meinhardt from *austriamicrosystems*, Unterpremstätten, Austria, who provided the Si/SiO_2 test specimens. Furthermore, we gratefully acknowledge financial support from Forschungsförderungsfonds für die gewerbliche Wirtschaft, Vienna, Austria, Max Kade Foundation, New York, NY, USA, and the Fonds zur Förderung der wissenschaftlichen Forschung, Vienna, Austria. Part of this work was done in the SFB "Elektroaktive Stoffe". Work at the NCEM was supported by the Director, Office of Energy Research, Office of Basic Energy Sciences, Materials Science Division of the U.S. Department of Energy under contract no. DE-AC03-76SF00098.

References

[1] R.F. Egerton, Electron Energy-Loss Spectroscopy in the Electron Microscope, Plenum Press, New York, 1996.
[2] H. Rose, E. Plies, Optik 40 (1974) 336.
[3] J. Bihr, G. Benner, D. Krahl, A. Rilk, E. Weimer, in: G.W. Bailey (Ed.), Proceedings of the 49th Annual Meeting on Electron Microsc. Soc. Amer., San Francisco Press, San Francisco, 1991, p. 354.
[4] M. Rühle, J.M. Mayer, J.C.H. Spence, J. Bihr, W. Probst, E. Weimer, Proceedings of the 49th Annual Meeting on Electron Microsc. Soc. Amer., San Francisco Press, San Francisco, 1991, p. 706.
[5] H. Shuman, A.V. Somlyo, D. Safer, T. Frey, A.P. Somlyo, Scann. Electron Microsc. (1985) 737.
[6] O.L. Krivanek, A.L. Gubbens, N. Dellby, Microsc. Microanal. Microstruct. 2 (1991) 315.
[7] D.A. Muller, Y. Tzou, R. Raj, J. Silcox, Nature 366 (1993) 725.
[8] W. Grogger, P. Warbichler, F. Hofer, T. Lang, W. Schintlmeister, Proceedings of the 14th International Congress on Electron Microscopy, vol. 1, 1998, p. 215.
[9] W.J. de Ruijter, J.K. Weiss, Rev. Sci. Instrum. 63 (1992) 4314.
[10] A. Berger, H. Kohl, Optik 92 (1993) 175.
[11] A. Berger, L. Mayer, H. Kohl, Ultramicroscopy 55 (1994) 101.
[12] G. Kothleitner, F. Hofer, Micron 29 (1998) 349.
[13] O.L. Krivanek, A.L. Gubbens, M.K. Kundmann, G.C. Carpenter, in: G.W. Bailey, C.L. Rieder (Eds.), Proceedings of the 51st EMSA Meeting, San Francisco Press, San Francisco, 1993, p. 586.
[14] D.E. Johnson, Introduction to Analytical Electron Microscopy, Plenum Press, New York, 1979, p. 245.
[15] P.A. Crozier, Ultramicroscopy 58 (1995) 157.
[16] F. Hofer, P. Warbichler, W. Grogger, Ultramicroscopy 59 (1995) 15.
[17] N. Bonnet, C. Colliex, C. Mory, M. Tence, in: A.M.F. O'Hare (Ed.), Scanning Microsc. Suppl., vol. 2, Scanning Microscopy Int., Chicago, 1988, p. 351.
[18] R.F. Egerton, Electron Energy-Loss Spectroscopy in the Electron Microscope, Plenum Press, New York, 1996.
[19] J. Bentley, J.E. Wittig, T.P. Nolan, Mater. Res. Soc. Symp. Proc. 517 (1998) 205.
[20] H. Shuman, C.F. Chang, A.P. Somlyo, Ultramicroscopy 19 (1986) 121.
[21] W.C. de Brujin, C.W.J. Sorber, E.S. Gelsema, A.L.D. Beckers, J.F. Jongkind, Scanning Microsc. 7 (1993) 693.
[22] F. Hofer, W. Grogger, G. Kothleitner, P. Warbichler, Ultramicroscopy 67 (1997) 83.
[23] K. Kimoto, J. Electron Microsc. 45 (1996) 143.
[24] R.F. Egerton, Ultramicroscopy 4 (1979) 169.
[25] R.D. Leapman, P. Rez, D.F. Mayers, J. Chem. Phys. 72 (1981) 1232.
[26] F. Hofer, Ultramicroscopy 21 (1987) 63.
[27] T. Malis, J.M. Titchmarsh, Inst. Phys. Conf. Ser. 78 (1986) 181.
[28] H. Kohl, A. Berger, Ultramicroscopy 59 (1995) 191.
[29] O.L. Krivanek, M.K. Kundman, K. Kimoto, J. Microsc. 180 (1995) 277.
[30] R.F. Egerton, J. Electron Microsc. 48 (1999) 711.
[31] T. Navidi-Kasmai, H. Kohl, Ultramicroscopy 81 (2000) 223.
[32] T. Terashima, Y. Bando, K. Iijima, K. Yamamoto, K. Hirata, K. Hayashi, K. Kamigaki, H. Terauchi, Phys. Rev. Lett. 65 (1990) 2684.
[33] I. Bozovic, J.N. Eckstein, MRS Bull. 20 (1995) 32.
[34] J.P. Loquet, A. Catana, E. Mächler, C. Gerber, J.G. Bednorz, Appl. Phys. Lett. 64 (1994) 372.
[35] T. Haage, Q.D. Jiang, M. Cardona, H.U. Habermeier, J. Zegenhagen, Appl. Phys. Lett. 68 (1996) 2427.

[36] S.J. Pennycook, M.F. Chisholm, D.E. Jesson, D.P. Norton, D.H. Lowndes, R. Feenstra, H.R. Kerchner, J.O. Thomson, Phys. Rev. Lett. 67 (1991) 765.
[37] C.L. Jia, H. Soltner, G. Jakob, T. Hahn, H. Adrian, K. Urban, Physica C 210 (1993) 1.
[38] M. Varela, Z. Sefrioui, D. Arias, M.A. Navacerrada, M. Lucia, M.A. Lopez de la Torre, C. Leon, G.D. Loos, F. Sanchez-Quesada, J. Santamaria, Phys. Rev. Lett. 83 (1999) 3936.
[39] M. Varela, W. Grogger, D. Arias, Z. Sefrioui, C. Leon, C. Ballesteros, K.M. Krishnan, J. Santamaria, Phys. Rev. Lett. 86 (2001) 5156.
[40] M. Varela, C. Ballesteros, W. Grogger, K.M. Krishnan, D. Arias, Z. Sefrioui, C. Leon, J. Santamaria, J. Alloys Comp. 323–324 (2001) 558.
[41] M. Varela, W. Grogger, D. Arias, Z. Sefrioui, C. Leon, L. Vazquez, C. Ballesteros, K.M. Krishnan, J. Santamaria, Phys. Rev. B 66 (2002) 174514.
[42] W. Grogger, F. Hofer, G. Kothleitner, Micron 29 (1998) 43.
[43] W. Grogger, K.M. Krishnan, R.A. Ristau, T. Thomson, S.D. Harkness, R. Ranjan, Appl. Phys. Lett. 80 (2002) 1165.
[44] W. Grogger, K.M. Krishnan, IEEE Trans. Magn. 37 (2001) 1465.
[45] B. Schaffer, Dipl. Thesis, Graz University of Technology, 2002.
[46] B. Schaffer, W. Grogger, F. Hofer, Micron 34 (2003) 1.
[47] S.J. Pennycook, Contemp. Phys. 23 (1982) 371.
[48] S.J. Pennycook, D.E. Jessen, A.J. McGibbon, P.D. Nellist, J. Electron Microsc. 45 (1996) 36.
[49] D.A. Muller, J. Silcox, Ultramicroscopy 59 (1995) 195.